A three-dimensional Gaussian-beam ray-tracing program for designing interferometer/polarimeter plasma diagnostics

George B. Warr[a] and John Howard[b]
Plasma Research Laboratory, Research School of Physical Sciences and Engineering, Institute of Advanced Studies, Australian National University, Canberra, ACT 0200, Australia

(Received 8 November 2000; accepted for publication 2 February 2001)

We have developed a three-dimensional Gaussian-beam ray-tracing program to aid in the design of infrared, far-infrared, and millimeter wave interferometer and polarimeter diagnostic systems for magnetic confinement fusion relevant plasma physics experiments. An overview of the program is presented along with a description of the ray-tracing algorithm. A model is developed for the case of diffraction of a Gaussian beam off a cylindrical grating and is shown to be in good agreement with experimental measurements. The program has been used to aid the design of the scanning-grating interferometer system for the H-1NF heliac experimental plasma device. The program is written in the Research Systems Inc. Interactive Data Language and, on a typical modern personal computer, is able to trace and render the ~50 element three-view 44-beam H-1NF interferometer optical system in about one minute. © *2001 American Institute of Physics.* [DOI: 10.1063/1.1361083]

I. INTRODUCTION

The design of interferometer and polarimeter diagnostic systems for magnetic confinement fusion relevant plasma physics experiments can be a complex task. As the plasma cross section in these experiments is often asymmetric, multichannel systems are required to deduce the density distribution.[1] Since these systems typically use infrared, far-infrared, or millimeter waves, a software design tool that takes account of the Gaussian nature of the beams and which accommodates specialized optical components such as cylindrical gratings is essential for the system design.

We report on a three-dimensional Gaussian-beam ray-tracing program (grt3d) we have developed to assist the design of the multiview tomographic interferometer system for the H-1NF heliac.[2,3] It has also been used to model the interferometer system on the compact helical system and to aid the design of the H-1NF 2 mm swept-frequency interferometer. The program is written in the Research Systems Inc. Interactive Data Language and has been used on unix workstations, personal computers (PCs), and macintosh desktop computers. On a typical modern PC the program is able to trace and render the H-1NF interferometer optical system in about a minute. The program includes a user friendly graphical user interface and a basic online help system. The software is freely available[4] to other researchers for use under the terms of the GNU General Public License.[5]

This article is organized as follows. An overview of the program is given in Sec. II, followed by sections describing how the optical elements are treated in the program. The geometry used in the program is illustrated with reference to a simple plane mirror (Sec. III) before considering the special case of Gaussian-beam reflection from the circumference of a cylindrical diffraction grating in Sec. IV. Other optical elements are discussed briefly in Sec. V. Results showing good agreement between the program model and experimental measurements are also presented in these sections. We conclude with a brief description of the complete H-1NF interferometer design and a comparison of the model predictions and experimental measurements for the beam paths.

II. GRT3D PROGRAM OVERVIEW

The three-dimensional Gaussian-beam ray-tracing program has three main windows for interaction with the user: (a) a system-viewer window where the optical system is rendered in three dimensions, (b) a beam-profile viewer that displays two-dimensional plots of the Gaussian-beam profiles throughout the optical system (see Fig. 1), and (c) a data-entry window where details about the optical system are specified.

Descriptions of the system optical components (i.e., position, orientation, aperture, focal length, etc.) are contained in an hierarchical tree structure. This facilitates the design of complex systems, allowing optical system subtrees to be easily added or removed. Optical elements can be positioned either relative to another system component or in absolute coordinates with respect to a user defined origin.

The ray-tracing algorithm used in the program traces ray paths from each source in the system until the beams are absorbed, either by an optical component, a detector, or at the system boundary. Some components, such as beam splitters and diffraction gratings, generate additional rays. These rays are traced by recursively calling the ray-tracing algorithm.

At each spatial increment the program calculates the properties of the Gaussian beam propagating along the ray between the components. Some optics, such as cylindrical

[a]Electronic mail: gbw112@rsphysse.anu.edu.au; http://www.rsphysse.anu.edu.au/~gbw112
[b]Electronic mail: John.Howard@anu.edu.au; http://wwwrsphysse.anu.edu.au/prl/staffcont/jnhcon.html

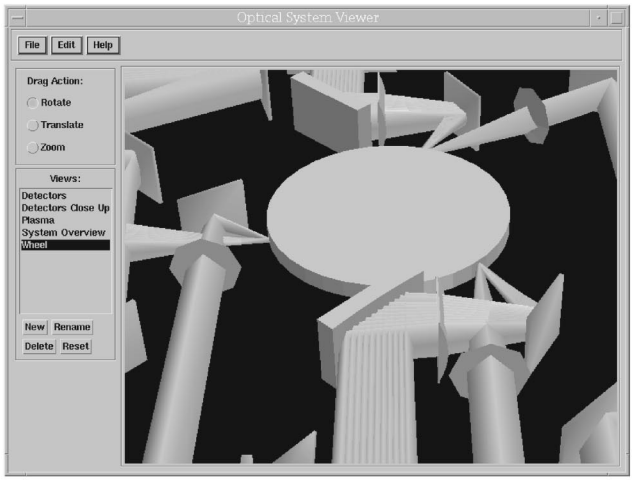

(a)

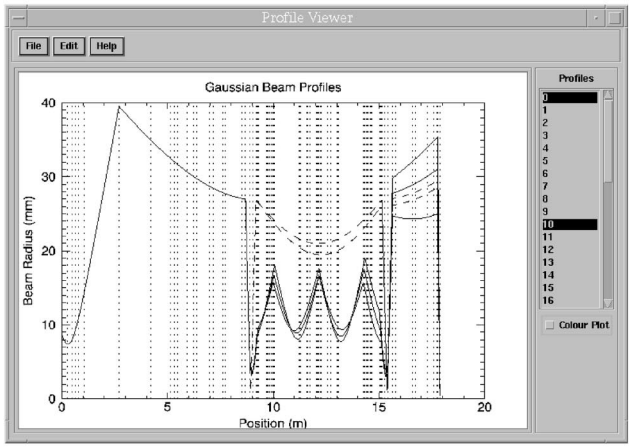

(b)

FIG. 1. Main windows of the ray-tracing program. (a) System-viewer window showing a close up of the grating wheel used in the H-1NF interferometer and (b) Gaussian-beam profile viewer showing beam profiles for one of the diagonal plasma probing views of the interferometer.

lenses alter the propagation behavior of the Gaussian beam in one plane only. To model such behavior the program maintains a coordinate system with unit vector **k** parallel to the ray direction and unit vectors **i** and **j** orthogonal to **k**, see Fig. 2. Gaussian-beam waist sizes w_0 and positions z_0 are computed for both the **i** and **j** components of the beam. The beam width (radius where the intensity $I=I_{\max}/e$) along the ray is calculated from the waist sizes and positions using the propagation equation

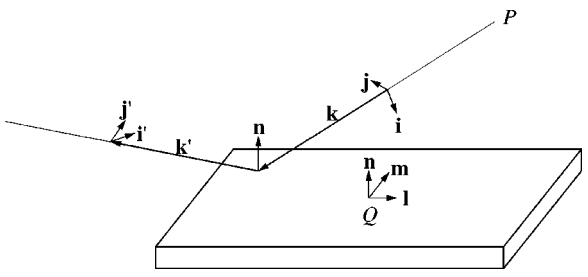

FIG. 2. Geometry for reflection of a ray off a plane mirror.

$$w(z)=w_0\left[1+\left(\frac{z-z_0}{z_R}\right)^2\right]^{1/2}, \tag{1}$$

where $z_R=k_0w_0^2$ (the Rayleigh length). The beam profiles viewer, Fig. 1(b), shows the profiles for the **i** (solid line) and **j** (dashed line) components of the beam. The dotted vertical lines in the figure indicate the positions where the beam intersects the optical components of the system. In this figure, profiles for the central and outer beams of a set of plasma probing beams for the H-1NF interferometer have been overplotted for comparison.

Currently polarization states are not traced by the program as it has been sufficient to model polarizers using beam splitters and plane mirrors. However, the fully three-dimensional approach to the beam propagation described above provides a natural basis for extension of the program to include polarization effects, using, for example, Jones matrices.

The program allows export of the rendered optical system in the data exchange file (DXF) and virtual reality modeling language (vrml) interchange formats for use in computer aided design programs and display on web pages.

III. PLANE MIRROR BEAM GEOMETRY

The geometry for a ray reflected off a plane mirror is shown in Fig. 2. A local coordinate system is maintained by the ray-trace program for each component in the optical system. For a mirror the local coordinate system origin is in the center of the front face of the mirror (point Q in the figure) and has orthogonal unit vectors **l** and **m** in the plane of the mirror and **n** the unit normal to the plane.

When a ray is reflected off the mirror the component of its wave vector in the direction of the mirror normal is opposite to that of the incident wave vector, $k_n'=-k_n$ so that

$$\mathbf{k}'=\mathbf{k}-2(\mathbf{k}\cdot\mathbf{n})\mathbf{n}. \tag{2}$$

The direction of the reflected unit vectors $\mathbf{i}'$ and $\mathbf{j}'$ used for maintaining the orthogonal components of the Gaussian beam, are similarly obtained.

IV. SCANNING ROTATING GRATING WHEEL

The use of a rotating cylindrical grating wheel to Doppler shift an incident monochromatic beam of radiation for heterodyne detection purposes was first proposed and demonstrated by Véron.[6] Howard[3] extended the concept to allow a scanning capability for the diffracted beam and presented a simple geometric optics analysis of the effect of the grating on the reflected beam profile parameters. This analysis is briefly summarized and adapted for Gaussian-beam propagation in Sec. IV A. Results confirming the reflection model are presented followed, in Sec. IV B, by an explanation of how the theory is implemented in the ray-tracing program.

A. Reflection of a Gaussian beam

The geometry of a typical scanning grating wheel is shown in Fig. 3. For beams propagating in the plane of the wheel the angles of incidence α and diffraction β are governed by the familiar grating equation

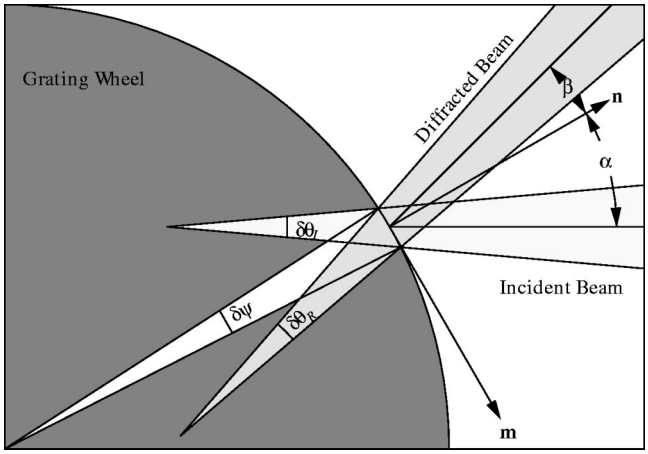

FIG. 3. Diffraction grating geometry showing the relationship between the incident and diffracted rays.

$$\sin\alpha+\sin\beta=m\lambda/d, \tag{3}$$

where m is the diffraction order, λ is the beam wavelength, and d is the spacing of the grating grooves.

The region the incident beam illuminates on the wheel is elliptical due to the inclination of the wheel surface to the beam. When the ratio of the incident beam diameter at the grating surface W_g to the wheel radius R is small the major axis of the ellipse is

$$a=W_g/\cos\alpha \tag{4}$$

which subtends an angle

$$\delta\psi=a/R \tag{5}$$

at the wheel center. The range of angles of incidence subtended at the wheel surface due to the incident beam convergence angle $\delta\theta_I$ is

$$\delta\alpha=\delta\psi-\delta\theta_I. \tag{6}$$

By simple geometry, the divergence angle of the diffracted beam is

$$\delta\theta_R=\delta\psi-\delta\beta, \tag{7}$$

where $\delta\beta$ is the range of angles of diffraction subtended at the wheel surface due to the diffracted beam divergence angle $\delta\theta_R$. Using the relationship

$$\delta\beta=-\frac{\cos\alpha}{\cos\beta}\delta\alpha \tag{8}$$

between the diffracted and incident angle differences in Eqs. (6) and (7) gives the divergence of the diffracted beam as

$$\delta\theta_R=(1+1/\mu)(\delta\psi-\delta\theta_I)+\delta\theta_I \tag{9}$$

with geometric factor

$$\mu=\cos\beta/\cos\alpha. \tag{10}$$

This analysis can be adapted to handle Gaussian beams by applying Eq. (9) to the local divergence (or convergence) angles $\delta\theta(z)$ of the incident and reflected beams at the grating surface and using the relationship between the incident and reflected beam radii at the grating: $w_g'=\mu w_g$ where the prime denotes the reflected beam. These two constraints enable determination of the diffracted beam waist radius and position which in turn define the propagation of the diffracted beam. The angle $\delta\theta(z)$ is defined through its relationship with the slope of the beam radius function $w(z)$:

$$\tan\left[\frac{\delta\theta(z)}{2}\right]\equiv\frac{dw(z)}{dz}=\frac{w_0}{z_R}\left[1+\left(\frac{z_R}{z-z_0}\right)^2\right]^{-1/2}. \tag{11}$$

$\delta\theta_I$ at the grating is determined using Eq. (11) and substituted into Eq. (9) to determine $\delta\theta_R$ at the grating. Substituting Eq. (11) for the diffracted beam into the Gaussian-beam propagation [Eq. (1)], gives the diffracted beam waist radius

$$w_0'=w_g'/\{1+[k_0w_g'\tan(\delta\theta_R/2)]^2\}^{1/2}. \tag{12}$$

The distance from the grating to the waist of the diffracted beam z_0' determined using these two equations is

$$z_0'=w_g'(k_0w_0')^2\tan(\delta\theta_R/2). \tag{13}$$

A negative value of z_0' indicates that the virtual waist is behind the grating surface and the diffracted beam is diverging, whereas a positive value of z_0' indicates the waist is after the grating and the diffracted beam is initially converging.

Figure 4 shows the good agreement of this theory to measured beam profiles. Shown are the effects on a dif-

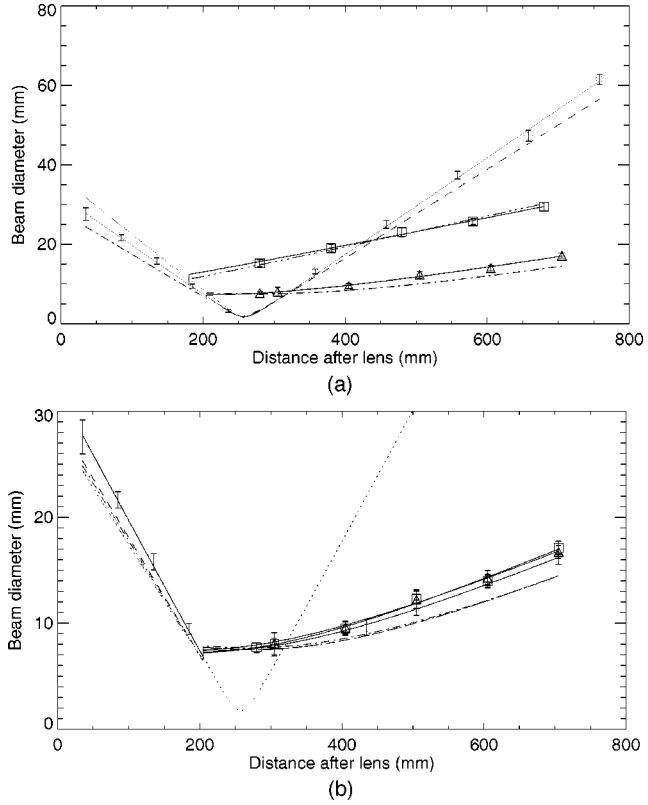

FIG. 4. Comparison of best fit to measured beam profiles (solid line) with predicted profiles (dashed line) for $\lambda=337\ \mu$m Gaussian beams diffracted off a 300 mm diameter grating wheel. The incident beam is focused by a $f=250$ mm hemispherical lens and is incident on the grating at $\alpha=30°$. Profiles are shown in (a) for fixed diffraction angle $\beta=10°$ and lens-grating separations of 180 mm □, 205 mm △, and 258 mm ◇, and in (b) for fixed lens-grating separation 205 mm and diffraction angles of $\beta=-10°$ □, $\beta=0°$ △, and $\beta=10°$ ◇. Uncertainties in the measurements are indicated by error bars. The dotted line in (b) shows the diffracted beam behavior in the orthogonal direction in which the grating behaves like a plane mirror.

fracted beam due to varying the distance between the grating and the converging incident beam (thereby changing $\delta\theta_I$ at the grating) and the effect of varying the diffraction angle β. As anticipated from Eq. (8) there is little effect on the diffracted beam profile for small changes in β. This is important for the proper functioning of the scanning-grating interferometer, where the diffracted beam angle is varied in order to effect a spatial scan of the plasma region. The diffracted beam behavior in the direction parallel to the grating grooves shown in Fig. 4(b), for which the grating behaves like a plane mirror, indicates the need for cylindrical correction optics to manage the elliptical nature of the diffracted beam.

B. Ray direction

In the general (noncoplanar) case, the direction of a beam diffracted off the grating wheel is determined using conservation of momentum. To this end, we let **n** normal to the wheel, **m** tangential to the wheel, and **l** parallel to the grating grooves define the local coordinate system at the point of intersection of the ray with the wheel and introduce the grating wave vector $\mathbf{k}_G = k_G\mathbf{m} = (2\pi m/d)\mathbf{m}$. The grating has no effect on the l component of the ray so $k_l' = k_l$. The component in the direction of **m** is given by momentum conservation

$$k_m' = k_m - k_G \tag{14}$$

[identical to Eq. (3)] while the component in the direction of **n** is obtained by energy conservation ($\|\mathbf{k}'\| = \|\mathbf{k}\|$) giving

$$k_n' = -k_n\left(1 + \frac{2k_m k_G - k_G^2}{k_n^2}\right)^{1/2}. \tag{15}$$

The diffracted wave vector is therefore

$$\mathbf{k}' = \mathbf{k} - \mathbf{k}_G - \left\{1 + \left[1 + \frac{2\mathbf{k}\cdot\mathbf{k}_G - \mathbf{k}_G^2}{(\mathbf{k}\cdot\mathbf{n})^2}\right]^{1/2}\right\}(\mathbf{k}\cdot\mathbf{n})\mathbf{n} \tag{16}$$

which reduces to the equation for specular reflection Eq. (2) when $\mathbf{k}_G = 0$.

V. OTHER OPTICS

The ray-trace program models a number of other optics. Routines have been written for cylindrical, cylindrical elliptic, cylindrical parabolic and spherical mirrors, cylindrical and spherical lenses, and beam splitters. The program can also calculate beam refraction on propagation through a plasma. In addition, common physical structures such as magnetic coils can be rendered to assist with the visualization of the optical system and its interference with external boundaries.

For the cylindrical, cylindrical elliptic, and cylindrical parabolic mirrors the reflected beam direction is determined using Eq. (2) taking **n** to be the surface normal at the point of intersection O of the incident ray with the surface (see Fig. 5). Provided the Gaussian-beam diameter $W = 2w$ is small compared to the focal length of the mirror and large compared to the wavelength of the radiation, Murphy[7] has shown that the geometric optics equation

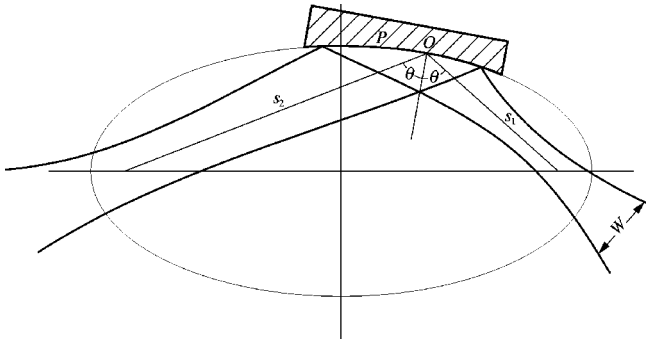

FIG. 5. Off-axis elliptical mirror geometry.

$$\frac{1}{f_O} = \frac{1}{s_1} + \frac{1}{s_2} \tag{17}$$

predicts the correct behavior of the transmission electron microscopy (TEM_{00}) component of the reflected beam to order $\epsilon_1 = W_m/(2f_O)$ and $\epsilon_2 = 2/(kW_m)$. Here W_m is the beam width on the mirror, $k = 2\pi/\lambda$, f_O is the local focal length at O and s_1 and s_2 are the distances from O to the foci of the ellipse. The power loss $1-\eta$ from the fundamental mode into higher modes is

$$1 - \eta = \frac{1}{2}\left(\frac{W_m}{f_O}\right)^2 \tan^2\theta, \tag{18}$$

where θ is the angle of incidence.

Figure 6 shows the good agreement of Eq. (17) with measurements of a HCN laser beam ($\lambda = 337\,\mu$m) reflected off a cylindrical parabolic mirror ($f_O = s_1, s_2 \to \infty$) for $s_1 = 300$, 400, and 500 mm. The values of W_m from Fig. 6 give $\epsilon_1 < 5\%$, $\epsilon_2 < 0.5\%$, and $\eta < 0.5\%$.

Cylindrical and spherical lenses have been used only on axis in the optical systems that we have modelled so this is the only case implemented in the program. In this case the ray direction is unaltered while the Gaussian nature of the

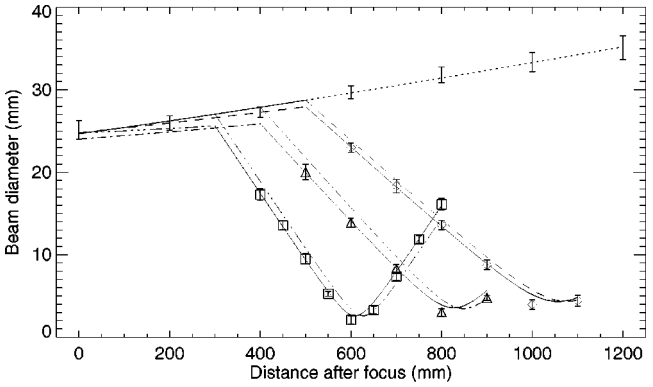

FIG. 6. Behavior of $\lambda = 337\,\mu$m Gaussian beams reflected off a cylindrical parabolic mirror. Solid lines indicate the best fit to the measured beam diameters. Dashed lines indicate profiles predicted by treating the mirror focal length $f = s_1$, the distance from the focus to the ray–mirror intersection point. □ $s_1 = 300$ mm, △ $s_1 = 400$ mm, ◇ $s_1 = 500$ mm. Uncertainties in the measurements are indicated by error bars. The mirror is designed so that $\theta = 45°$ at $s_1 = 400$ mm. The dotted line shows the reflected beam behavior in the orthogonal direction for which the mirror behaves like a plane mirror.

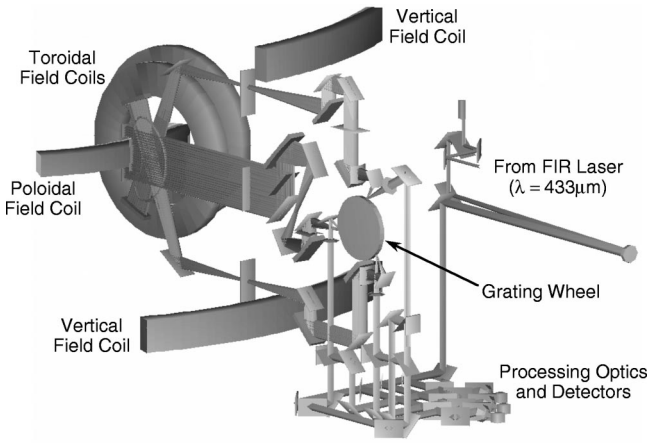

FIG. 7. Optical system for the H-1NF interferometer.

beam is changed according to the well known relations derived by Véron[6] for the transmitted beam waist distance from the lens d_{t0} and radius w_{t0},

$$d_{t0}=f+\frac{(d_{i0}-f)f^2}{z_R^2+(d_{i0}-f)^2}, \tag{19}$$

$$w_{t0}=\frac{fw_{i0}}{[(d_{i0}-f)^2+z_R^2]^{1/2}}. \tag{20}$$

Here f is the focal length of the lens and d_{i0} and w_{i0} are the incident beam waist distance from the lens and radius, respectively.

The refraction of a beam as it propagates through a plasma is calculated by steeping the beam through a simulated plasma profile and determining the ray direction and position at each step due to the gradient in the profile. If at the ith step the ray direction is $\mathbf{k}_i$ and ray position is $\mathbf{r}_i$, their values at the next step are given by $\mathbf{k}_{i+1}=\mathbf{k}_i+h\mathbf{K}_i$ and $\mathbf{r}_{i+1}=\mathbf{r}_i+h\mathbf{k}_i$, where

$$\mathbf{K}_i=\frac{\nabla\mu(\mathbf{r}_i)-[\mathbf{k}_i\cdot\nabla\mu(\mathbf{r}_i)]\mathbf{k}_i}{\mu(\mathbf{r}_i)} \tag{21}$$

is the change in ray direction, μ is the plasma refractive index for the beam (for example, $\mu=\mu_0$ for a beam propagating in the ordinary mode), and h is the step size.

This refraction part of the program was initially written as a separate program and includes an algorithm to trace Stokes vectors as the beam propagates allowing determination of Faraday rotation angles for polarized beams.

VI. COMPARISON OF GRT3D WITH MEASUREMENTS OF THE H-1NF INTERFEROMETER OPTICAL SYSTEM

The optical system for the H-1NF interferometer is shown in Fig. 7. It is comprised of five interferometer subsystems: two interferometers with sets of beams which probe the plasma diagonally from above and below, another two interferometers with sets of beams which probe the plasma horizontally (one set above the other), and a reference interferometer.

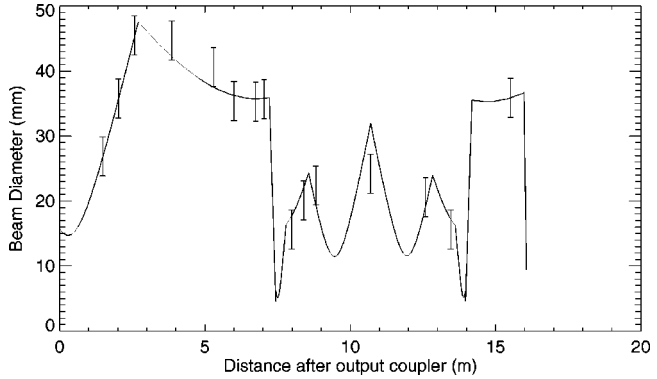

FIG. 8. Comparison of the beam diameter determined by the ray-tracing program (solid line) with experimental measurements. Uncertainties in the measurements are indicated by error bars. The profile is for the central beam of the H-1NF interferometer which diagonally probes the plasma from below. The component of the beam tangential to the grating wheel is shown.

Figure 8 compares the beam profile predicted by grt3d with experimental measurements of the profile width for the central beam of the interferometer which diagonally probes the plasma from below. Apart from the positions and specifications of the optical elements, only the initial beam waist width and position for the 433 μm optically pumped far-infrared (OPFIR) laser source [determined by fitting the propagation Eq. (1) to measurements of the beam profiles after the source] were supplied to grt3d. The good agreement between the predicted and measured beam profiles shows that the program can be used confidently to design optical systems.

ACKNOWLEDGMENTS

Thanks are due to D. Giddings for his help in writing the interface for input of the optical system elements. This work was in part supported by the Australian Institute of Nuclear Science and Engineering, the Australian Research Council, and the Australian Vice-Chancellors' Committee Commonwealth Scholarship and Fellowship Plan.

[1] A. J. H. Donné, Rev. Sci. Instrum. **66**, 3407 (1995).
[2] G. B. Warr, B. D. Blackwell, J. Wach, and J. Howard, Fusion Eng. Des. **34–35**, 387 (1997).
[3] J. Howard, Rev. Sci. Instrum. **61**, 1086 (1990).
[4] See http://www.rsphysse.anu.edu.au/~gbw112/grt3d.
[5] *GNU general public license*, Free Software Foundation Incorporated (1991) [The GNU General Public License can also be found on the internet at http://www.fsf.org/copyleft/gpl.html].
[6] D. Véron, in *Infrared and Millimeter Waves*, edited by K. J. Button (Academic, New York, 1979), Vol. 2, Chap. 2, pp. 67–135.
[7] J. A. Murphy, Int. J. Infrared Millim. Waves **8**, 1165 (1987).